2008

Computational simulation of separated flow in a three-dimensional diffuser using v2-f and zeta-f models

Jason Allen Ryon
Iowa State University

Computational simulation of separated flow in a three-dimensional diffuser using $\overline{v^2} - f$ and $\zeta - f$ models

by

Jason Allen Ryon

A thesis submitted to the graduate faculty

in partial fulfillment of the requirements for the degree of

MASTER OF SCIENCE

Major: Aerospace Engineering

Program of Study Committee:
Paul Durbin, Major Professor
Tom I-Ping Shih
Hui Hu

Iowa State University

Ames, Iowa

2008

DEDICATION

I would like to dedicate this thesis to my wife Amanda without whose support I would not have been able to complete this work. I would also like to thank my friends and family for their loving guidance and support.

TABLE OF CONTENTS

LIST OF TABLES

LIST OF FIGURES

ACKNOWLEDGEMENTS

I would like to take this opportunity to express my thanks to those who helped me with various aspects of conducting research and the writing of this thesis. First and foremost, Dr. Paul Durbin for his guidance, patience and support throughout this research and the writing of this thesis. I would additionally like to thank the Technical Manager: Dr. Chunill Hah, NASA-Glenn, as well as Dr. Ali Ameri, Dr. David Rigby, and Mr. Elbert Jeyapaul for their guidance throughout this research. I would also like to thank my committee members for their efforts and contributions to this work: Dr. Tom I-P Shih and Dr. Hui Hu. Special thanks also to Mr. Jim Wellman, Dr. James Coyle, and Mr. John Dickerson for their support. This work was sponsored by NASA Grant No. NNX07AB29A.

ABSTRACT

Computational prediction of separated flows is an area of interest, specifically in applications to gas turbine engines, liquid pumps, and many other engineering applications. Although these types of flows are governed by the Navier-Stokes equations, direct numerical simulation (DNS) of practical engineering flows is currently too expensive in terms of the required computational time. It is therefore a case to attempt simulation of these flows using the Reynolds-Averaged Navier-Stokes (RANS) equations which must be closed by utilizing a turbulence closure model.

The present study used the NASA Glenn-HT code, a compressible Navier-Stokes solver, with two different turbulence models, the $\overline{v^2}-f$ model of Durbin and the $\zeta-f$ model of Hanjalić, to observe their abilities to predict separated flows. The elliptic relaxation turbulence models and their implementation in Glenn-HT are described. Three cases are described to show the ability and limitations of these turbulence models.

CHAPTER 1. OVERVIEW

Computational prediction of separated flows is an area of interest, specifically in applications to gas turbine engines, liquid pumps, and many other engineering applications. Although these types of flows are governed by the Navier-Stokes equations, direct numerical simulation (DNS) of practical engineering flows is currently too expensive in terms of the required computational time. It is therefore a case to attempt simulation of these flows using the Reynolds-Averaged Navier-Stokes (RANS) equations which must be closed by utilizing a turbulence closure model.

The objective of this study was to employ two different turbulence models, namely the $\overline{v^2}-f$ model of Durbin and the $\zeta-f$ model of Hanjalić, and to observe their abilities to predict separated flows. Calculations were performed using the NASA Glenn-HT code, a compressible Navier-Stokes solver. The previously implemented $\overline{v^2}-f$ model and the newly implemented $\zeta-f$ model were both formulated in an implicit scheme which was solved using the GMRES iterative matrix solver. Three experimental cases were considered and the computational and experimental results were compared.

This thesis begins with a brief overview of turbulence modeling using eddy viscosity models, followed by motivation and description of the elliptic relaxation turbulence models, specifically $\overline{v^2}-f$ and $\zeta-f$ models. There is also a concise description of the Glenn-HT code along with details involving the implementation of turbulence models. Finally, the three cases and their numerical results are discussed.

CHAPTER 2. METHODS

2.1 Turbulence Modeling

Turbulence is defined by Durbin (2004) as the highly irregular flow of fluids, and is governed by the exact, Navier-Stokes, momentum equations. Although direct numerical simulation (DNS) of turbulent flows is possible, it is impractical for flows of interest because of the excessive computational requirements. In order to reduce the computational expense, the Reynolds-averaged Navier-Stokes (RANS) equations are employed. They require the addition of a turbulence model to achieve closure. Two eddy viscosity models, the $\overline{v^2} - f$ elliptic relaxation model of Durbin, and a similar $\zeta - f$ model of Hanjalić, have shown very promising results in previous cases (Ameri, Ajmani 2004, Hanjalić, *et. al.* 2004, Durbin 1995) and have been shown to accurately predict heat transfer, skin friction, and boundary layer separation.

This chapter gives a brief introduction into Reynolds-Averaging of the Navier-Stokes equations, eddy viscosity modeling, specifically elliptic relaxation models, and also the equations which constitute the $\overline{v^2} - f$ and $\zeta - f$ models. In addition, a brief overview of the Glenn-HT code and implementation of the $\zeta - f$ model will be given; a complete description can be found at Steinthorsson, *et. al.* (1999).

2.1.1 Reynolds-Averaged Navier-Stokes Equations

The momentum and continuity equations govern (Newtonian) viscous flows

$$\partial_t \rho \tilde{u}_i + \partial_j \rho \tilde{u}_j \tilde{u}_i = -\partial_i \tilde{p} + \partial_j [\mu \left(\partial_i \tilde{u}_j + \partial_j \tilde{u}_i \right)] \tag{2.1}$$

$$\partial_t \rho + \partial_j \rho \tilde{u}_j = 0 \tag{2.2}$$

The idea of Reynolds Decomposition is that a random variable $\tilde{u}$ can be represented as the sum of it's mean and fluctuating parts

$$\tilde{u} = U + u \tag{2.3}$$

Averaging is denoted by an overbar. Then $U \equiv \bar{\tilde{u}}$ and the fluctuation u is defined to be the turbulence. At low Mach number, compressibility of the turbulence equations can be ignored, while it is maintained in the mean flow equations.

The Reynolds Decomposition Equation 2.3 is substituted into the Navier-Stokes Equations 2.1 and 2.2 and the result is the Reynolds-averaged Navier-Stokes (RANS) equations.

$$\overline{\rho}\partial_t U_i + \overline{\rho} U_j \partial_j U_i = -\partial_i P + \partial_j[\overline{\mu}\,(\partial_i U_j + \partial_j U_i)] - \partial_j(\overline{\rho}\ \overline{u_j u_i}) \tag{2.4}$$

$$\partial_t \bar{\rho} + \partial_j \overline{\rho} U_j = 0 \tag{2.5}$$

The last term in the averaged momentum equation, Equation 2.4, is a derivative of the Reynolds stress tensor, which represents the averaged turbulent convection. To further investigate this Reynolds stress term, the fluctuating velocity equation can be written by subtracting the RANS Equations 2.4 and 2.5 from the Navier-Stokes Equations 2.1 and 2.2

$$\partial_t u_i + U_k \partial_k u_i + u_k \partial_k U_i + \partial_k(u_k u_i - \overline{u_k u_i}) = -\frac{1}{\rho}\partial_i p + \nu \nabla^2 u_i \tag{2.6}$$

Further manipulation (described in Durbin, Reif 2001) reveals the equation for the Reynolds stress transport

$$\partial_t \overline{u_i u_j} + U_k \partial_k \overline{u_i u_j} = \mathcal{P}_{ij} + \wp_{ij} - \frac{2}{3}\varepsilon\delta_{ij} + T_{ij} + \frac{1}{\rho}\partial_k(\mu \partial_k \overline{u_i u_j}) \tag{2.7}$$

where the terms $\mathcal{P}_{ij}$, $\wp_{ij}$, ε, and T_{ij} are named production, redistribution, dissipation, and turbulent transport, respectively. These terms are defined as

$$\mathcal{P}_{ij} \equiv -\overline{u_j u_k}\partial_k U_i - \overline{u_i u_k}\partial_k U_j \tag{2.8}$$

$$\wp_{ij} \equiv \frac{1}{\rho}\left(-\overline{u_j \partial_i p} - \overline{u_i \partial_j p} + \frac{2}{3}\delta_{ij}\overline{u_k \partial_k p}\right) - 2\nu\overline{\partial_k u_i \partial_k u_j} + \frac{2}{3}\delta_{ij}\varepsilon \tag{2.9}$$

$$\varepsilon \equiv \nu\overline{\partial_k u_j \partial_k u_j} \tag{2.10}$$

$$T_{ij} \equiv -\left(\partial_k \rho \overline{u_k u_i u_j} + \frac{2}{3\rho}\delta_{ij}\overline{u_k \partial_k p}\right) \tag{2.11}$$

The equation for turbulent kinetic energy is one-half the trace of Equation 2.7

$$\partial_t \rho k + U_j \partial_j \rho k = \rho \mathcal{P} - \rho\varepsilon - \left[\partial_j\left(\overline{u_j p} + \frac{1}{2}\rho\overline{u_j u_i u_i}\right) + \partial_i(\mu\partial_i k)\right] \tag{2.12}$$

The mean rate of strain tensor is

$$S_{ij} = \frac{1}{2}\left(\partial_i U_j + \partial_j U_i\right) \tag{2.13}$$

The rate of production of turbulent kinetic energy is

$$\rho\mathcal{P} = 2\mu_t S_{ij} S_{ji} - \frac{2}{3}\rho k \partial_i U_i - \frac{2}{3}\mu_t\left(\partial_i U_i\right)^2 = 2\mu_t |S|^2 - \frac{2}{3}\rho k\left(\nabla \cdot U\right) - \frac{2}{3}\mu_t\left(\nabla \cdot U\right)^2 \tag{2.14}$$

The mean flow equations, Equations 2.4 and 2.5, are unclosed because these 4 equations have 10 unknowns (P, U_i, and the addition of the Reynolds stress tensor components $\overline{u_i u_j}$ for $i = 1, 2, 3, j \leq i$). The goal of turbulence models is to provide closure to the RANS Equations 2.4 and 2.5. Turbulence models provide statistics of the complex, eddying motion to the mean flow equations so the mean flow field can be predicted without the need to directly simulate every detail of the flow. Using an additional set of relatively simple equations with empiricisms for closure, an eddy viscosity μ_t is predicted, which is related to the mean flow equations, 2.4 and 2.5. A number of turbulence models, from simple algebraic models to more complex Second Moment Closure (SMC) and Elliptic-Relaxation models can be found in Durbin, Reif (2001) and Wilcox (1994).

2.1.2 $\overline{v^2} - f$ Model

The most widely used turbulence models today consist of two-equation eddy viscosity models, commonly the $k - \varepsilon$ and $k - \omega$ models. Elliptic relaxation models alter the near-wall behavior of these two-equation models by solving an elliptic equation, instead of the normal near-wall treatment.

The $\overline{v^2} - f$ model of Durbin introduces $\overline{v^2}$ as a "wall-normal" velocity scale. A transport equation for this velocity scalar replaces the Reynolds stress tensor. Also, an elliptic relaxation

term, f, which is similar to a redistribution term, is used to sensitize $\overline{v^2}$ to the wall effect. Although this model does not compute the complete stress field that is needed for flows with secondary circulations, it is a better option than standard $k-\varepsilon$ models, since it retains the near-wall stress anisotropy which allows for accurate prediction of heat transfer, skin friction, and boundary layer separation in turbulent flows (Durbin, Reif 2001).

The $\overline{v^2}-f$ model is characterized by the familiar transport equations for k and ε as shown in Equations 2.15 and 2.16.

$$\partial_t(\rho k)+U_j\partial_j(\rho k)=\rho\mathcal{P}-\rho\varepsilon+\partial_j\left[\left(\mu+\frac{\mu_t}{\sigma_k}\right)\partial_j k\right] \tag{2.15}$$

$$\partial_t(\rho\varepsilon)+U_j\partial_j(\rho\varepsilon)=\frac{C_{\varepsilon1}\rho\mathcal{P}-C_{\varepsilon2}\rho\varepsilon}{T}+\partial_j\left[\left(\mu+\frac{\mu_t}{\sigma_\varepsilon}\right)\partial_j\varepsilon\right] \tag{2.16}$$

The transport equation for the velocity scalar $\overline{v^2}$ is given as

$$\partial_t\left(\rho\overline{v^2}\right)+U_j\partial_j\left(\rho\overline{v^2}\right)=\rho k f-\frac{\rho\overline{v^2}\varepsilon}{k}+\partial_k\left[\left(\mu+\frac{\mu_t}{\sigma_{\overline{v^2}}}\right)\partial_k\overline{v^2}\right] \tag{2.17}$$

An elliptic equation for f, which brings in the effect of the walls, is given by

$$L^2\nabla^2 f-f=-c_2\frac{\mathcal{P}}{k}+\frac{c_1}{T}\left(\frac{\overline{v^2}}{k}-\frac{2}{3}\right) \tag{2.18}$$

Boundary conditions for no-slip walls are given for the four equations as

$$k_w=0,\varepsilon_w=\lim_{y\to0}\left(\frac{2\nu k}{y^2}\right),\overline{v^2}_w=0,f_w=lim_{y\to0}\left(\frac{-20\nu^2\overline{v^2}}{\varepsilon y^4}\right) \tag{2.19}$$

where y denotes the distance to the wall of the first cell center. The turbulent time scale, T, with realizability constraints, is reformulated for this model as

$$T=min\left[max\left[\frac{k}{\varepsilon},C_T\sqrt{\frac{\nu}{\varepsilon}}\right],\frac{\alpha k}{\sqrt{3}\,\overline{v^2}C_\mu|S|}\right] \tag{2.20}$$

Similarly, the turbulent length scale is

$$L=min\left[C_L max\left[\frac{k^{3/2}}{\varepsilon},C_\eta\left(\frac{\nu^3}{\varepsilon}\right)^{1/4}\right],\frac{1}{\sqrt{6}}\frac{k^{3/2}}{C_\mu\overline{v^2}\sqrt{S^2}}\right] \tag{2.21}$$

Finally, the eddy viscosity, which is communicated to the mean flow equations, is computed as

$$\mu_t=C_\mu\rho\overline{v^2}T \tag{2.22}$$

One aspect of the $\overline{v^2}-f$ model is, unlike Reynolds stress models, Equations 2.15 and 2.16 can be solved uncoupled from Equations 2.17 and 2.18, which aids convergence. As with all eddy viscosity models, empirical constants must be used. Table 2.1 gives these constants.

c_1	c_2	C_L	C_T	C_η	$C_{\varepsilon 1}$	$C_{\varepsilon 2}$	C_μ	α	σ_k	σ_ε	$\sigma_{\overline{v^2}}$
0.4	0.3	0.3	6.0	70.0	$1.3+\frac{1}{4\left[1+(y/2L)^2\right]^4}$	1.92	0.19	0.6	1.0	1.3	1.0

Table 2.1 Constants for $\overline{v^2}-f$ Model

2.1.3 $\zeta - f$ Model

According to Hanjalić, *et. al.* (2004), the $\overline{v^2}-f$ model's treatment of the wall boundary for f, as shown in Equation 2.19, is computationally inefficient as it is sensitive to near-wall grid clustering. Therefore, Hanjalić proposed a similar model, the $\zeta - f$ model, with the goal of reducing the computational sensitivity by solving a transport equation for the velocity scales ratio $\zeta = \overline{v^2}/k$ instead of the transport equation for $\overline{v^2}$. This model improves numerical stability and robustness and reduces the sensitivity to near-wall grid clustering.

As in the $\overline{v^2}-f$ model, the k and ε equations are given as Equations 2.23 and 2.24

$$\partial_t(\rho k) + U_j\partial_j(\rho k) = \rho\mathcal{P} - \rho\varepsilon + \partial_j\left[\left(\mu + \frac{\mu_t}{\sigma_k}\right)\partial_j k\right] \tag{2.23}$$

$$\partial_t(\rho\varepsilon) + U_j\partial_j(\rho\varepsilon) = \frac{C_{\varepsilon 1}\rho\mathcal{P} - C_{\varepsilon 2}\rho\varepsilon}{T} + \partial_j\left[\left(\mu + \frac{\mu_t}{\sigma_\varepsilon}\right)\partial_j\varepsilon\right] \tag{2.24}$$

The transport equation for ζ is given by substituting $\zeta = \overline{v^2}/k$ into Equation 2.17

$$\partial_t(\rho\zeta) + U_j\partial_j(\rho\zeta) = \rho f - \frac{\rho\zeta\mathcal{P}}{k} + \partial_k\left[\left(\mu + \frac{\mu_t}{\sigma_\zeta}\right)\partial_k\zeta\right] + X \tag{2.25}$$

Here X is the cross diffusion term caused by the transformation and can be written as

$$X = \frac{2}{k}\left(\mu + \frac{\mu_t}{\sigma_\zeta}\right)\partial_k\zeta\partial_k k \tag{2.26}$$

In Hanjalić, *et. al.* (2004), the X is omitted in Equation 2.25 because the term is not significant, except close to the wall. To account for this omission, some of the coefficients were re-tuned. An elliptic equation for f is given as

$$L^2\nabla^2 f - f = \frac{1}{T}\left(c_1 + c_2\frac{\mathcal{P}}{\varepsilon}\right)\left(\zeta - \frac{2}{3}\right) \tag{2.27}$$

Boundary conditions for the no-slip walls are given for the four equations as

$$k_w = 0, \varepsilon_w = \lim_{y\to 0}\left(\frac{2\nu k}{y^2}\right), \zeta_w = 0, f_w = \lim_{y\to 0}\left(\frac{-2\nu\zeta}{\varepsilon y^2}\right) \tag{2.28}$$

Note that the value for f_w is more convenient compared with the f_w of the $\overline{v^2} - f$ model. The denominator of f_w is proportional to y^2 instead of y^4, which is larger as $y \to 0$ and improves numerical stability. The turbulent time scale, T, is given as

$$T = max\left[min\left[\frac{k}{\varepsilon}, \frac{\alpha}{\sqrt{6}C_\mu\zeta|S|}\right], C_T\sqrt{\frac{\nu}{\varepsilon}}\right] \tag{2.29}$$

Similarly, the turbulent length scale, L, is represented by

$$L = C_L max\left[min\left[\frac{k^{3/2}}{\varepsilon}, \frac{k^{1/2}}{\sqrt{6}C_\mu\zeta|S|}\right], C_\eta\left(\frac{\nu^3}{\varepsilon}\right)^{1/4}\right] \tag{2.30}$$

The solution to these three transport equations and one elliptic equation leads to a field of eddy viscosity

$$\mu_t = C_\mu\rho\zeta kT \tag{2.31}$$

The coefficients required by this model, which account for the omission of the cross diffusion, X, are given in Table 2.2

c_1	c_2	C_L	C_T	C_η	$C_{\varepsilon 1}$	$C_{\varepsilon 2}$	C_μ	α	σ_k	σ_ε	σ_ζ
0.4	0.65	0.36	6.0	85.0	$1.4\,(1 + 0.012/\zeta)$	1.9	0.22	0.6	1.0	1.3	1.2

Table 2.2 Constants for $\zeta - f$ Model

2.2 Description of Glenn-HT

The Glenn-HT code is described by Steinthorsson, *et. al.* (1999) to be "designed for detailed and accurate simulations of turbomachinery flows and heat transfer that are aimed at understanding the physical phenomena involved and evaluation of relevant physical models." This code will be briefly described in the present work; a much more detailed description is found at Steinthorsson, *et. al.* (1999).

Three important design choices found in any CFD code are (i) structure, (ii) discretization, and (iii) time stepping scheme. These choices, along with a brief description of the implementation of turbulence models will be described.

2.2.1 Grid Structure

Glenn-HT uses a *locally* structured but *globally* unstructured *multiblock* grid system. Structured grids are those whose gridpoints are arranged in a regular fashion, allowing the cells of each block to be arranged in a sequential array. These structured blocks are then placed adjacent to other blocks, leading to the multiblock grid system. The grid is considered to be globally unstructured because of the ability to patch faces of adjacent blocks together but allow for the presence of *mesh singularities* where, in two dimensions, three, five or more block corners (or edges in three dimensions) come together. The resulting grid structure allows for very complex geometries to be used.

A simple grid generator was written to generate the grids for the present study. This grid generator used a two-surface method in the y-direction and z-direction to create smooth grids. In addition, it allowed for clustering near no-slip walls. It also provided simple grid decomposition for use on multi-processor computers.

2.2.2 Discretization

The continuity equation, Equation 2.5, the momentum equation, Equation 2.4, as well as the total energy equation which is found in Steinthorsson, *et. al.* (1999) are solved by Glenn-HT. These equations were discretized by finite volumes. The finite volume approach writes the governing equations in integral form for each cell of the grid. Solutions are found for mass, momentum, and total energy at cell centers and the fluxes through the cell faces are computed. The solutions are integrated in time using an explicit multi-stage scheme, constructed by Jameson, Schmidt, and Turkel. The discretized equations are marched in time to a steady state using a fourth order Runge-Kutta time stepping scheme.

2.2.3 Nondimensionalization

The governing equations were nondimensionalized using a set of reference conditions, along with the Prandtl number, which is taken to be constant

$$p_{ref}$$

$$T_{ref}$$

$$\mu_{ref}$$

$$Pr = \frac{\mu c_p}{k} \tag{2.32}$$

From the reference conditions, derived reference quantities were calculated

$$\begin{aligned} \rho_{ref} &= \frac{p_{ref}}{RT_{ref}} \\ c_{ref} &= \sqrt{\frac{\gamma p_{ref}}{\rho_{ref}}} \\ u_{ref} = \sqrt{RT_{ref}} &= \frac{c_{ref}}{\sqrt{\gamma}} \\ t_{ref} &= \frac{L}{u_{ref}} \end{aligned} \tag{2.33}$$

Using the reference variables, the nondimensional quantities were defined as

$$\begin{aligned} \tilde{p} &= p/p_{ref} \\ \tilde{T} &= T/T_{ref} \\ \tilde{L} &= L/L_{ref} \\ \tilde{\rho} &= \rho/\rho_{ref} \\ \tilde{c} &= c/c_{ref} \\ \tilde{u} &= u/u_{ref} \\ \tilde{t} &= t/t_{ref} \end{aligned} \tag{2.34}$$

Also, a *Code Reynold's Number*, Re_{code}, is defined as

$$Re_{code} \equiv \frac{u_{ref} L_{ref}}{\nu_{ref}} \tag{2.35}$$

2.2.4 Implementation of Turbulence Models

Turbulence models that were previously implemented in Glenn-HT include the Baldwin-Lomax model , the $k-\omega$ model of Wilcox, and Durbin's $\overline{v^2}-f$ models. The present work implemented the $\zeta-f$ model of Hanjalić. The reason for the implementation of the $\overline{v^2}-f$ and

$\zeta - f$ models is their ability to accurately predict heat transfer, skin friction, and boundary layer separation in turbulent flows.

The turbulence equations were decoupled from the mean flow equations and solved in an implicit manner. In the $\overline{v^2} - f$ and $\zeta - f$ models, the k and ε equations were solved coupled together, but uncoupled from the $\overline{v^2}$ (and ζ) and f equations, which were also solved in a coupled manner. These two sets of coupled equations were solved with an iterative matrix solver, GMRES, and the turbulent viscosity μ_t was calculated and related to the mean flow equations.

In both the $\overline{v^2} - f$ and $\zeta - f$ models, the diffusion terms were discretized with second order central differences. The convective terms were discretized using first order upwind differences. An explicit discretization was used for the source terms. Also, multigrid is not used for the turbulence equations, although it can be used in the mean flow calculations.

2.2.5 Recirculating Boundary Condition

Another addition to the Glenn-HT code was the ability to recirculate flow from the exit back into the inlet, as well as the ability to read in velocity profiles into the inlet boundary. These additions allowed for a channel flow to be run, with recirculation, to produce a fully turbulent velocity profile which could then be read into other cases which required this type of inlet boundary condition.

CHAPTER 3. CASE 1: 2-DIMENSIONAL CHANNEL FLOW

A simple channel flow was computed to validate that the implementation of the $\zeta - f$ model was correct. This case was run with the Glenn-HT code with two turbulence models, Durbin's $\overline{v^2} - f$ Model, and Hanjalić's $\zeta - f$ model. The purpose of this case was to determine if $\zeta - f$ was properly implemented by comparing the results to separate, 1-D, solutions for channel flow.

3.1 Description

A channel that measured 1 cm in height by 150 cm in length was run with a bulk inlet velocity of around 1 m/s at a Reynold's number of 10,000. The top and bottom sides were set as no-slip walls, and the side walls were set as slipping walls, thus the flow was 2-D.

3.2 Grid

A grid was created using an in-house grid generator. This grid consisted of 8 blocks, and each block had 17 gridpoints in the x-direction and 65 gridpoints in the y-direction. The z-direction was kept at 5 gridpoints because the flow is two-dimensional. The side walls were allowed to slip, while the top and bottom walls were set as a no-slip boundary. The grid was clustered near the no-slip walls so the first cell from the wall had a $y_+ \approx 1$. Figures 3.1 and 3.2 show closeup 3-D and side views of the grid.

3.3 Numerical Results

The case was computed with both the $\overline{v^2} - f$ and $\zeta - f$ turbulence models. Figures 3.3 and 3.4 show the fully-developed streamwise velocity profiles from the wall to the centerline

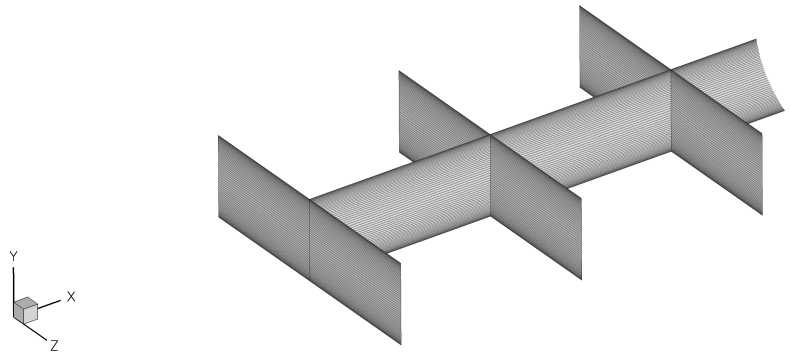

Figure 3.1 Case 1: Numerical Grid 3-D View

Figure 3.2 Case 1: Numerical Grid Side View

compared with the 1-D solution for the $\overline{v^2} - f$ and $\zeta - f$ models, respectively. Both models predict the velocity profiles well.

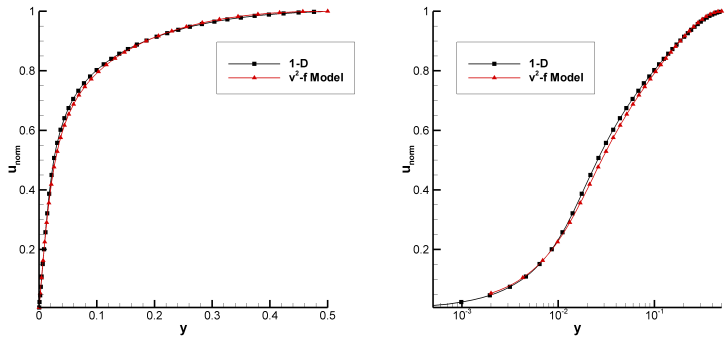

Figure 3.3 Case 1: Streamwise Velocity Profile with $\overline{v^2} - f$ Model

3.4 Summary

The implementation of the $\overline{v^2} - f$ and $\zeta - f$ models in Glenn-HT were validated against a separate, 1-D, solution for a simple channel flow. Both the $\overline{v^2} - f$ and $\zeta - f$ models performed

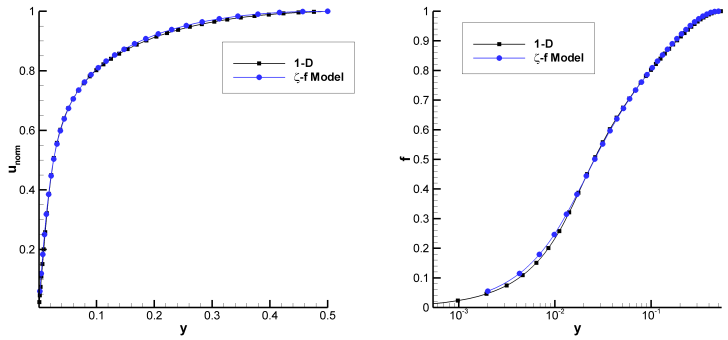

Figure 3.4 Case 1: Streamwise Velocity Profile with $\zeta - f$ Model

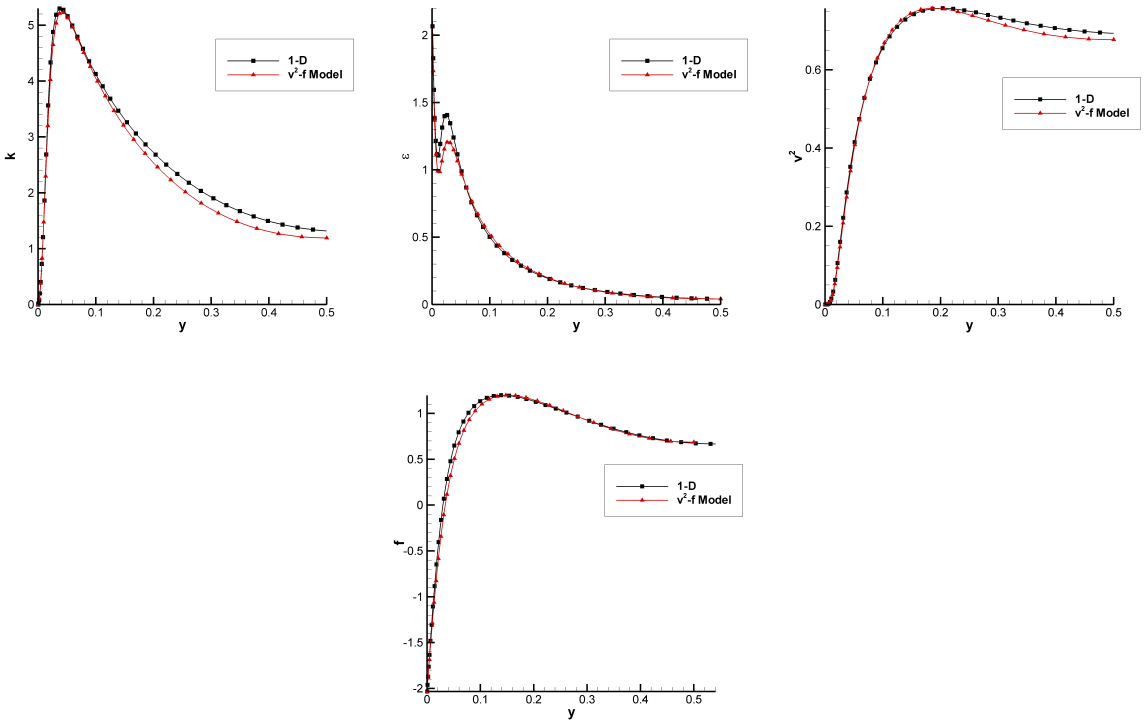

Figure 3.5 Case 1: Turbulence Quantities with $\overline{v^2} - f$ Model

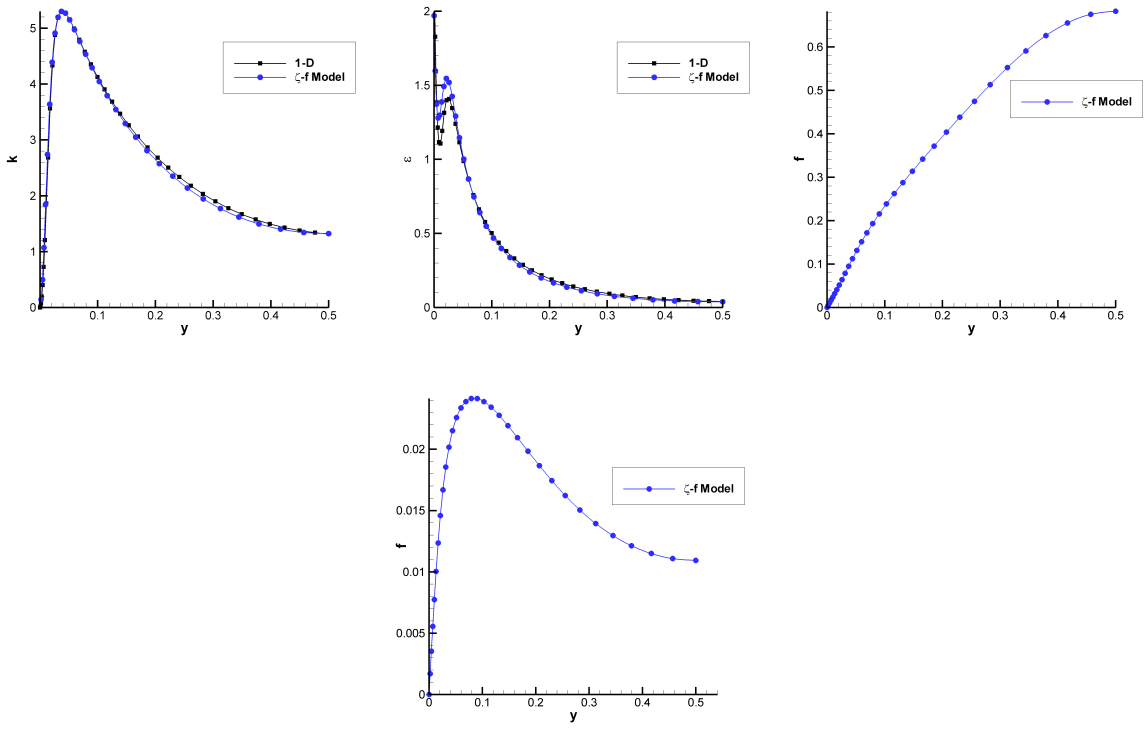

Figure 3.6 Case 1: Turbulence Quantities with $\zeta - f$ Model

well and accurately predicted the velocity profile as well as the turbulence quantities.

CHAPTER 4. CASE 2: 3-DIMENSIONAL DIFFUSER - SINGLE SLANTING WALL

A 3-D diffuser with one sloping wall and three straight walls was simulated with Glenn-HT to display the abilities of the $\overline{v^2} - f$ and $\zeta - f$ models to predict separated flows.

4.1 Description

A diffuser with an inlet of 1 cm x 3.33 cm was sloped along the top wall at an angle of 11.3°. The length of the diffuser was 15 cm, and the outlet section that was 4 cm x 3.33 cm. Upstream of the diffuser section, a straight development channel was included, as well as a straight channel after the outlet of the diffuser, which was followed by a converging section. The converging section was necessary because Glenn-HT cannot handle separated flow in the outlet boundary. This case does not correspond to an experiment, but was intended to be a simplified version of the 3-D diffuser with two slanting walls which is described in the next chapter. Therefore, only conceptual results can be concluded for this case. The Reynold's number based off of the inlet height was 10,000. The inlet bulk velocity was 1 m/s.

4.2 Grid

A grid was created with approximately 1.5 million gridpoints using an in-house grid generator. This grid consisted of 20 blocks, and each block had 17 gridpoints in the x-direction and 65 gridpoints in the y-direction and z-direction. The grid was clustered near the walls in the y-direction and z-direction so the first cell from the wall had a $y_+ \approx 1$. Clustering was also used in the x-direction to ensure the majority of gridpoints were located in the diffuser section, which was the primary area of interest. Figures 4.1, 4.1, 4.3, and 4.4 show the 3-D

view, side view, top view, and diffuser inlet and exit slices, respectively. The inlet section was kept short because a separate channel flow simulation was run to be fully developed and this fully developed velocity profile was used as the inlet boundary condition for the present case.

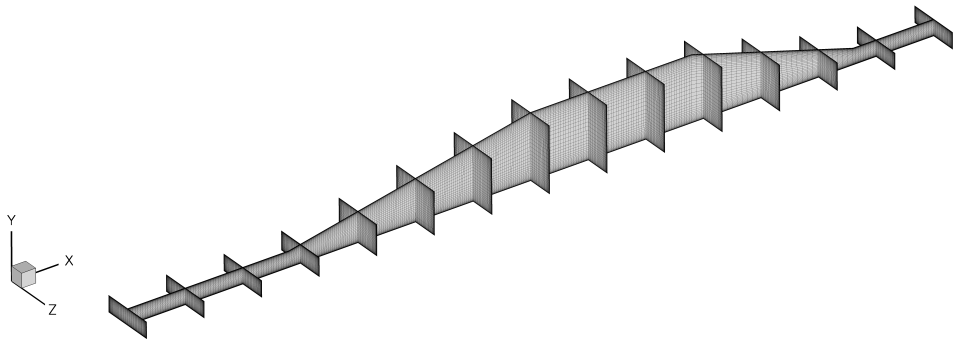

Figure 4.1 Case 2: Numerical Grid 3-D View

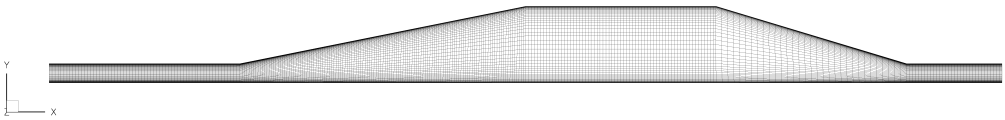

Figure 4.2 Case 2: Numerical Grid Side View

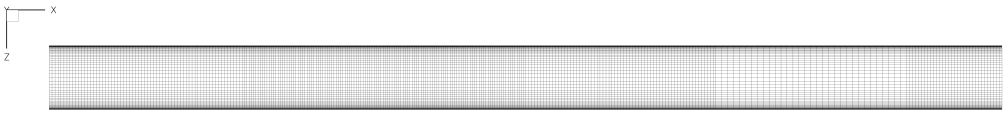

Figure 4.3 Case 2: Numerical Grid Top View

4.3 Numerical Results

The first step of this simulation was to determine the boundary conditions. The inlet was a fully developed channel flow and the sides, top and bottom walls were all set to no-slip boundary conditions. The non-dimensionalized parameters needed by Glenn-HT were the same

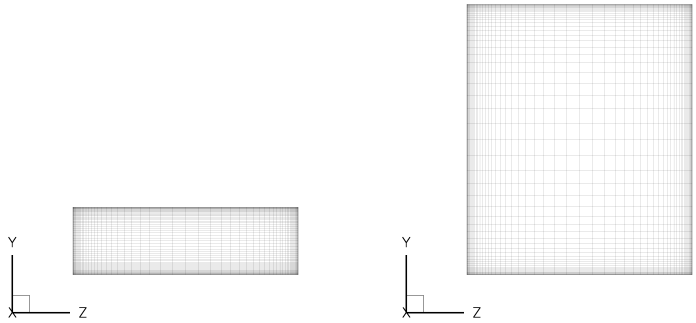

Figure 4.4 Case 2: Numerical Grid Diffuser Inlet and Exit Slice

as the 3-D diffuser with two sloping walls and are described in the next chapter and listed in Tables 5.1 and 5.2.

The case was run on Iowa State University's "Lightning Cluster" with both the $\overline{v^2} - f$ and $\zeta - f$ models. Figures 4.5 and 4.6 show an isosurface of slightly negative streamwise velocity to show the location of separation. All velocities shown were normalized by the bulk inlet velocity.

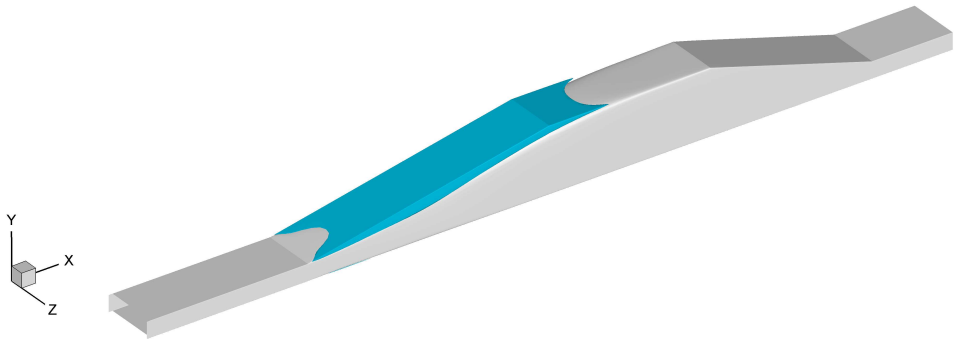

Figure 4.5 Case 2: Isosurface of Separation with $\overline{v^2} - f$ Model

Figures 4.7 and 4.8 show slices of streamwise velocity contours at x = 0 cm, 1 cm, 2 cm, 4 cm, 8 cm, and 12 cm for the $\overline{v^2} - f$ and $\zeta - f$ models, respectively. Also, Figures 4.9 and 4.10 show a contours of streamwise velocity at the longitudinal midspan, z = 1.6667 cm, for both turbulence models.

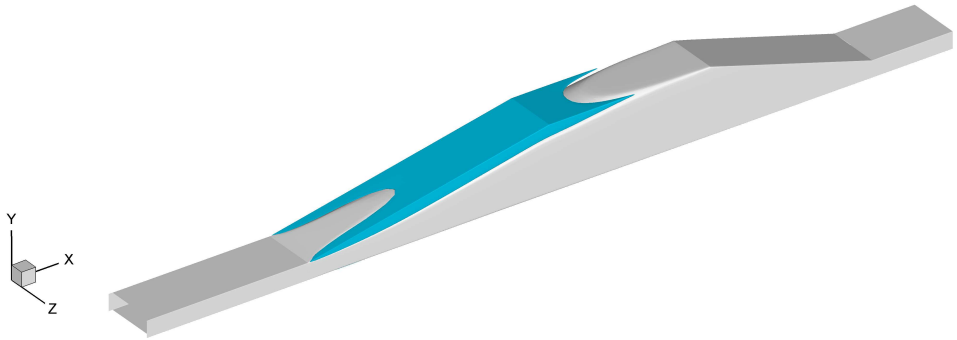

Figure 4.6 Case 2: Isosurface of Separation with $\zeta - f$ Model

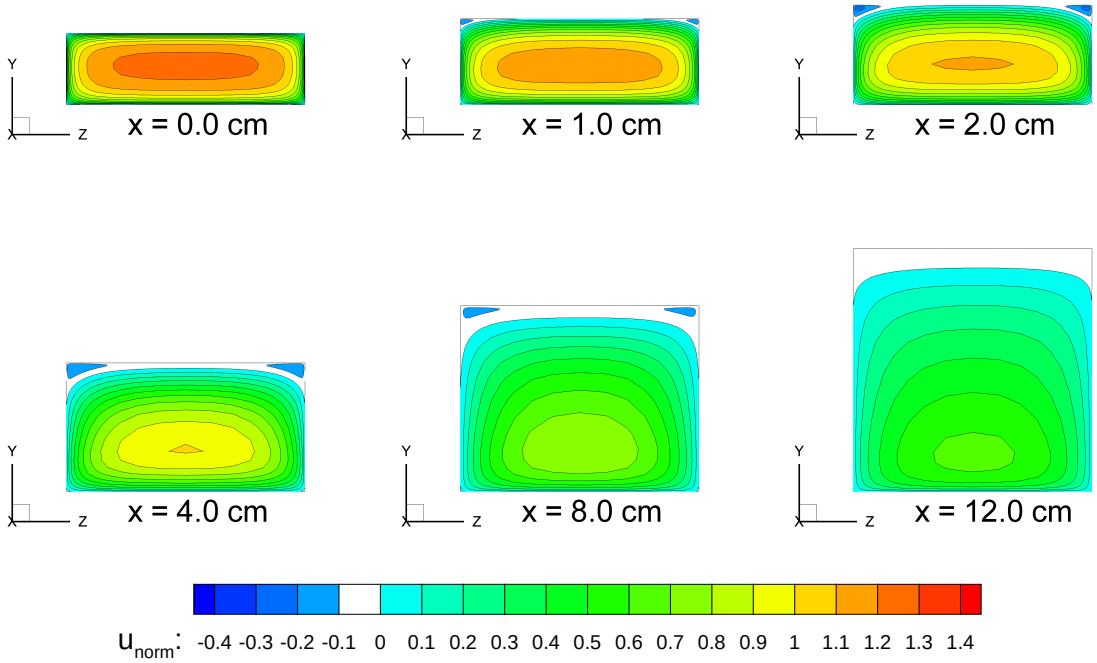

Figure 4.7 Case 2: Contours of Streamwise Velocity with $\overline{v^2} - f$ Model

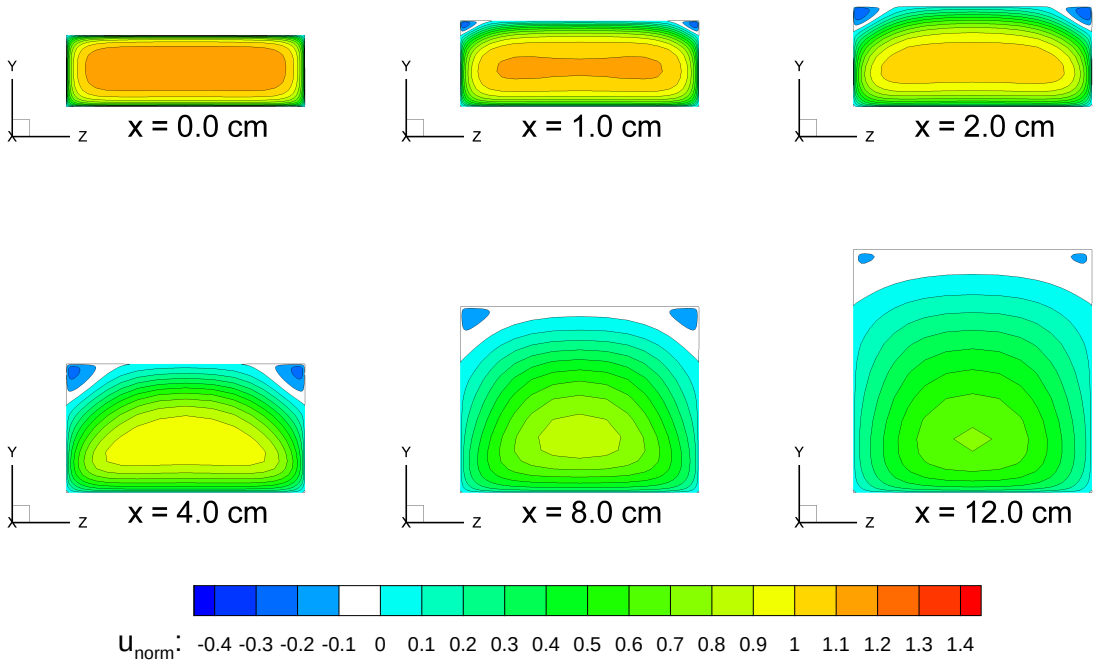

Figure 4.8 Case 2: Contours of Streamwise Velocity with $\zeta - f$ Model

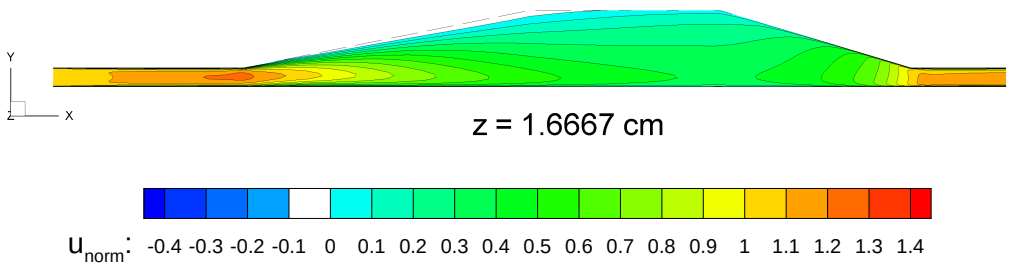

Figure 4.9 Case 2: Contours of Streamwise Velocity at the Longitudinal Midspan with $\overline{v^2} - f$ Model

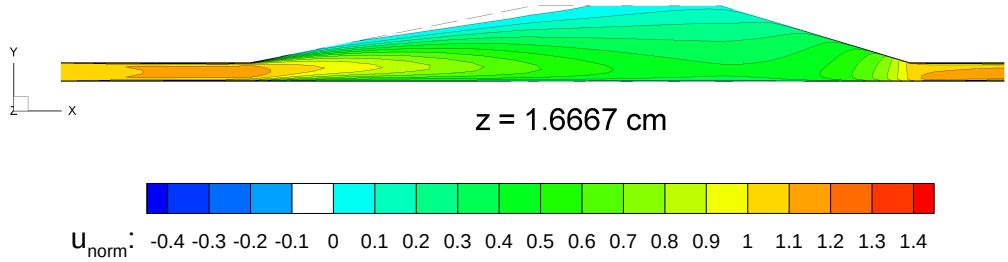

Figure 4.10 Case 2: Contours of Streamwise Velocity at the Longitudinal Midspan with $\zeta - f$ Model

4.4 Summary

While experimental data was not available for this case, the conceptual results can be described. Three concepts are concluded about this test case. First, the symmetry about the centerline in the z-direction resulted in a flow that was symmetrical, including the separated area. Next, since only the top wall was sloping, it was expected and also found to be true that the separation would occur along this sloped wall. This is consistent with previous studies of 2-D diffusers. The third conclusion that was made about this diffuser was that the no-slip side walls influenced the separation near the top edges. Both the $\overline{v^2} - f$ and $\zeta - f$ models predicted the onset of separation at the top right and left edges. The separation continued across the top sloped wall and eventually reattached.

CHAPTER 5. CASE 3: 3-DIMENSIONAL DIFFUSER

Separated flow in a 3-D diffuser was recently studied in an experiment conducted by Cherry *et. al.* (2006). The objective of this experiment was to provide a 3-D diffuser with simple geometry, well-specified boundary conditions, and a well-defined 3-D recirculation region which was challenging for numerical models to predict.

5.1 Description

The experiment consisted of a 15 cm long diffuser that expanded along one side at 2.54°, and also expanded along the top side at 11.3° while the remaining side and bottom walls remain straight. This resulted in an expansion ratio of 4.8. The inlet of the diffuser was 1 cm x 3.33 cm and the exit was a 4 cm x 4 cm square outlet. Figures 5.1, 5.2, and 5.3 show the 3-D, top, and side views of this geometry. Upstream of the diffuser section was a long (60 cm) development channel that created a fully developed channel flow. The exit of the diffuser was connected to a 10 cm straight outlet channel followed by a converging section.

The working fluid of the experiment was water and the diffuser had a bulk inlet velocity of 1 m/s. The Reynolds number based off of the diffuser inlet height was 10,000.

5.2 Experimental Results

The velocity data was collected using the method of magnetic resonance velocimetry (MRV) which provided the three-component mean velocity vectors. Figure 5.4 shows an isosurface of slightly negative u-velocity, which clearly shows separation beginning near the start of the diffuser, at the top right corner. Separation soon moves to cover the top side. Slices of streamwise velocity contours are shown in Figure 5.5 at x = 0 cm, 1 cm, 2 cm, 4 m, 8 cm, and

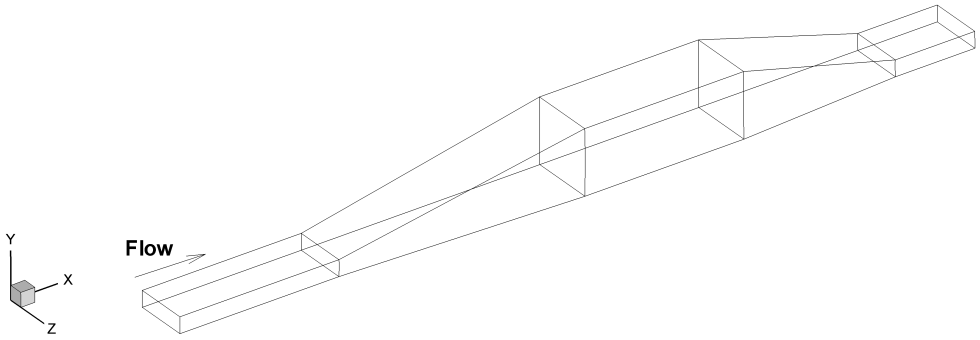

Figure 5.1 Case 3: Geometry 3-D View

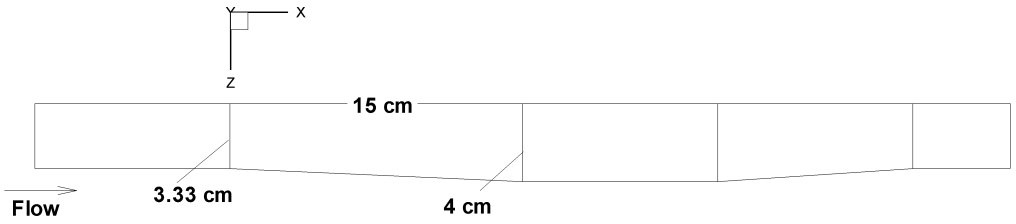

Figure 5.2 Case 3: Geometry Top View

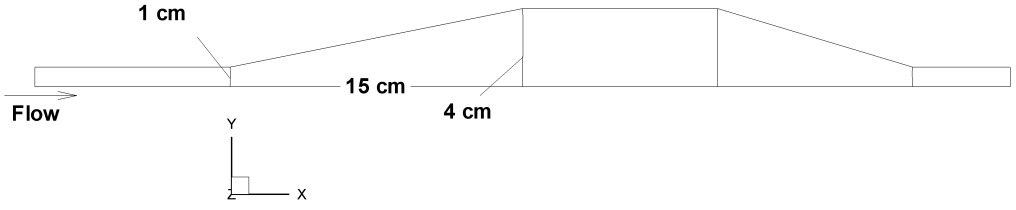

Figure 5.3 Case 3: Geometry Side View

12 cm. Also, a slice at z = 2 cm is shown in Figure 5.6. All velocities shown were normalized by the bulk inlet velocity.

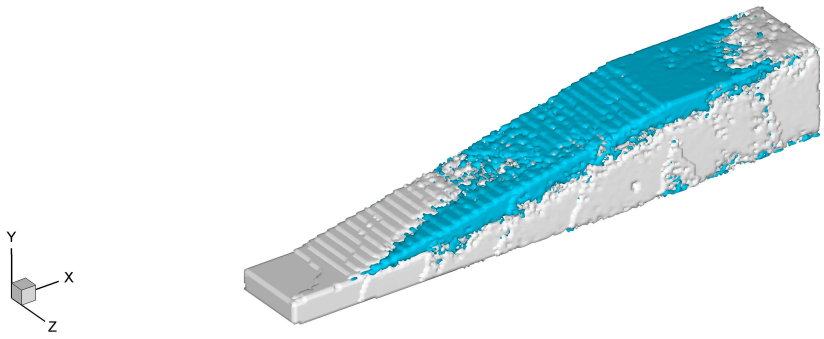

Figure 5.4 Case 3: Experimental Isosurface of Separation

5.3 Grid

A grid was created with approximately 1.5 million gridpoints using an in-house grid generator. This grid consisted of 20 blocks, and each block had 17 gridpoints in the x-direction and 65 gridpoints in the y-direction and z-direction. The grid was clustered near the walls in the y-direction and z-direction so the first cell from the wall had a $y_+ \approx 1$. Clustering was also used in the x-direction to ensure the majority of gridpoints were located in the diffuser section, which was the primary area of interest. Figures 5.7, 5.7, 5.9, and 5.10 show the 3-D view, side view, top view, and diffuser inlet and exit slices, respectively. The grid consists of a short inlet section, a diffuser section, straight diffuser exit section, a converging nozzle, and a short exit extension. The straight diffuser exit section, converging section, and exit extensions were added to ensure that the exit boundary condition did not contain reversed flow, which cannot be handled by the Glenn-HT outlet boundary. Also, the inlet section was kept short because a separate channel flow simulation was run to be fully developed and this fully developed velocity profile was used as the inlet boundary condition for the present case.

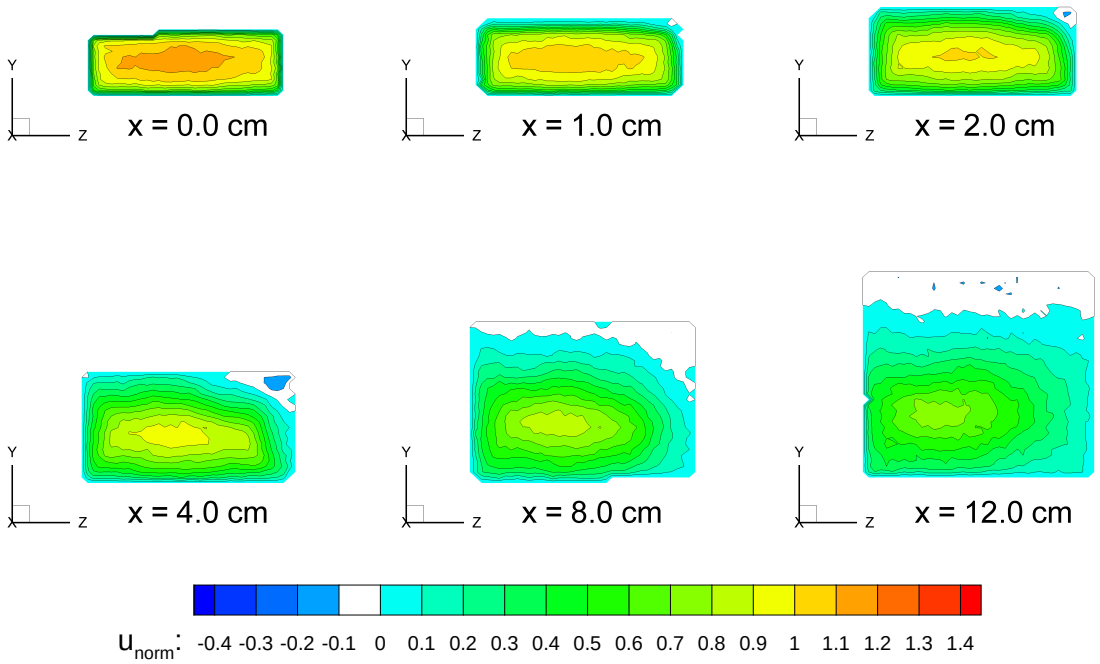

Figure 5.5 Case 3: Experimental Contours of Streamwise Velocity

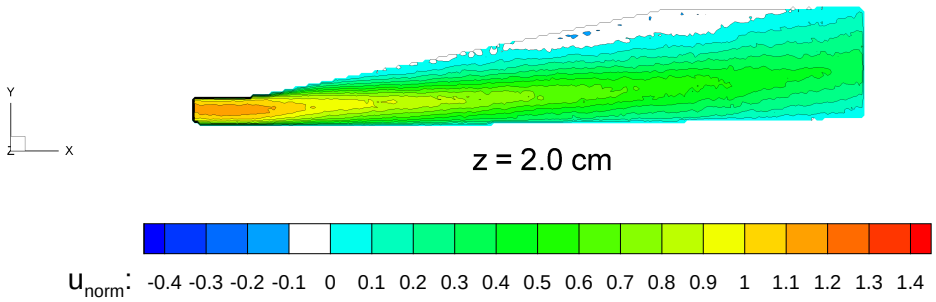

Figure 5.6 Case 3: Experimental Contours of Streamwise Velocity at z = 2 cm

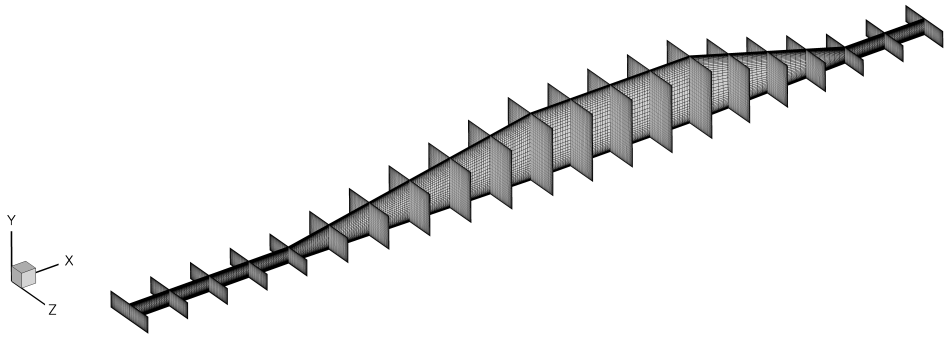

Figure 5.7 Case 3: Numerical Grid 3-D View

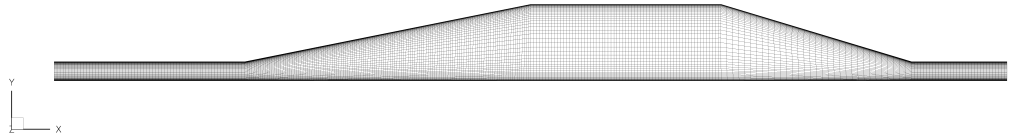

Figure 5.8 Case 3: Numerical Grid Side View

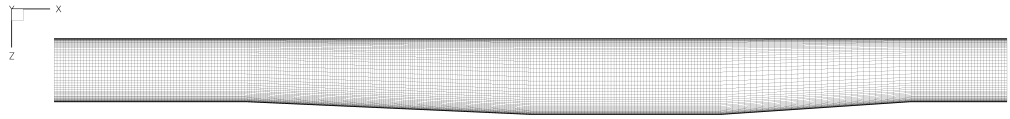

Figure 5.9 Case 3: Numerical Grid Top View

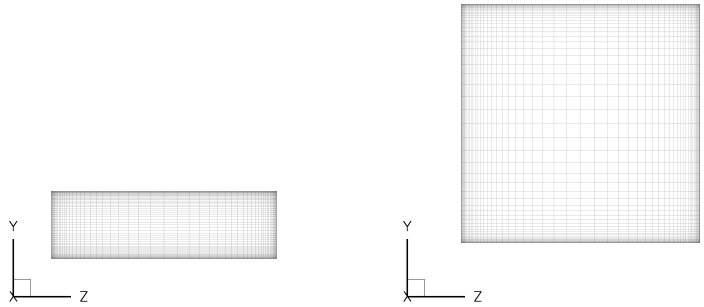

Figure 5.10 Case 3: Numerical Grid Diffuser Inlet and Exit Slice

5.4 Numerical Results

Using the Glenn-HT code, two separate simulations were run. The first simulation used the $\overline{v^2} - f$ model, and the second used the $\zeta - f$ model.

The first step in setting up this case was to determine the boundary conditions. While maintaining the same Reynold's number as the experiment, the working fluid was changed from water to air, which is the working fluid used by the Glenn-HT solver. To account for the change in viscosity, the velocity, u, was increased to maintain the same Reynold's Number.

$$Re_{exp} = \frac{uL}{\nu_{water}} = \frac{(1m/s)\,(0.01m)}{1.004 \times 10^{-6} m^2/s} \approx 10,000 \tag{5.1}$$

where u is the velocity, L is the reference length chosen as the height of the channel, and ν is the kinematic viscosity.

$$Re_{cfd} = \frac{uL}{\nu_{air}} = \frac{(15.1m/s)\,(0.01m)}{1.51 \times 10^{-5} m^2/s} \approx 10,000 \tag{5.2}$$

The other reference variables required for non-dimensionalization are listed in Table 5.1

Reference Variable	Corresponding Variable	Value
Reference Pressure, p_{ref}	Inlet Total Pressure, p_t	$101,325Pa$
Reference Temperature, T_{ref}	Inlet Total Temperature, T_t	$293K$
Reference Length, L_{ref}	Channel Height	$0.01m$
Reference Viscosity, ν_{ref}	Kinematic Viscosity of Air, ν_{air}	$1.51 \times 10^{-5} m^2/s$

Table 5.1 Case 3: Reference Variables

Reference Variable	Corresponding Variable	Value
Reference Density, ρ_{ref}	$\frac{p_{ref}}{RT_{ref}}$	$1.2049kg/m^3$
Reference Speed of Sound, c_{ref}	$\sqrt{\frac{\gamma p_{ref}}{\rho_{ref}}}$	$343m/s$
Reference Velocity, u_{ref}	$\sqrt{R_{ref}T_{ref}}$	$289.98m/s$
Reference Time, t_{ref}	$\frac{L_{ref}}{u_{ref}}$	$3.45 \times 10^{-5}s$
Reference Reynold's Number, Re_{ref}	$\frac{u_{ref}L_{ref}}{\nu_{ref}}$	192,039

Table 5.2 Case 3: Derived Reference Variables

Compressible codes have convergence problems at low speeds. To maintain the incompressible nature and still allow for adequate convergence, the velocity, u, and viscosity, ν, were both

scaled equally by a factor s, which comes into play in the Reynold's number, Re_{ref}. This allows the code to be run at a speed of $u \approx 100m/s$, which is still incompressible.

$$\nu_{ref} = \nu_{ref} \times s = 1.02 \times 10^{-4}$$
$$Re_{ref} = \frac{u_{ref} L_{ref}}{s\nu_{ref}} = 28,429 \tag{5.3}$$

with $s = 6.755$. Note that Re_{ref} is based off of u_{ref} and not u. The value of u was scaled by s while u_{ref}, which is used only for nondimensionalization, was not scaled.

The Glenn-HT boundary conditions were created using the non-dimensionalized values as described in Equation 2.34, and can be seen in Table 5.3. Note that the outlet in Glenn-HT is after the converging section, and not the outlet of the diffuser. The case was run on Iowa

Inlet:
Inlet Temperature, $\tilde{T} = 1.0$
Total Pressure, $\tilde{p} = 1.0$
Inlet Flow Angles $= 0°$
Inlet Mach Number, $M_{in} = 0.3$
Outlet:
Static Pressure, $p_{out} = .9$
Outlet Mach Number, $M_{out} = 0.3$
Walls:
No-Slip Walls

Table 5.3 Case 3: Boundary Conditions

State University's "Lightning Cluster" with both the $\overline{v^2} - f$ and $\zeta - f$ models. Figures 5.11 and 5.12 show an isosurface of slightly negative streamwise velocity to show the location of separation.

Figures 5.13 and 5.14 show slices of streamwise velocity contours at x = 0 cm, 1 cm, 2 cm, 4 cm, 8 cm, and 12 cm for the $\overline{v^2} - f$ and $\zeta - f$ models, respectively. Also, Figures 5.15 and 5.16 show a contours of streamwise velocity at z = 2 cm for both turbulence models.

5.5 Summary

A quantitative comparison between the experimental and computational results makes evident that the computational simulations show the onset of separation the same location, the

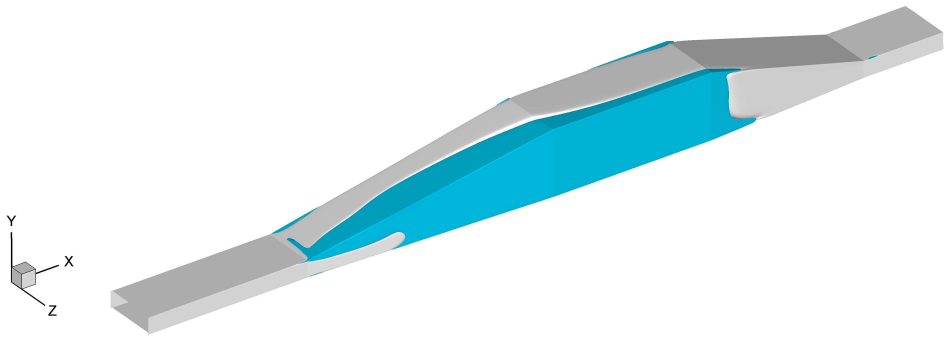

Figure 5.11 Case 3: Isosurface of Separation with $\overline{v^2} - f$ Model

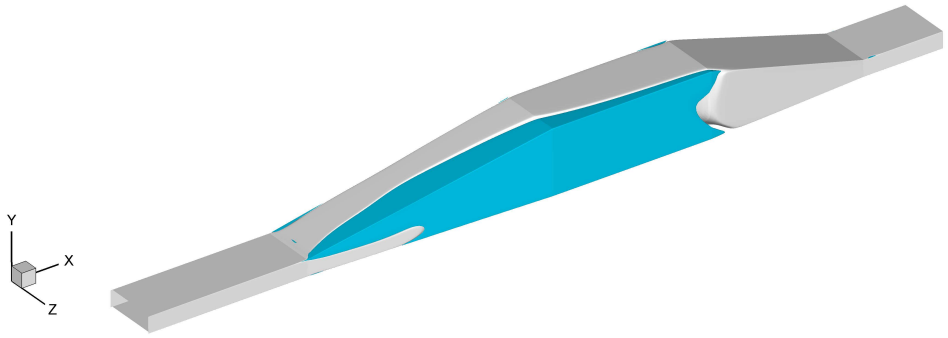

Figure 5.12 Case 3: Isosurface of Separation with $\zeta - f$ Model

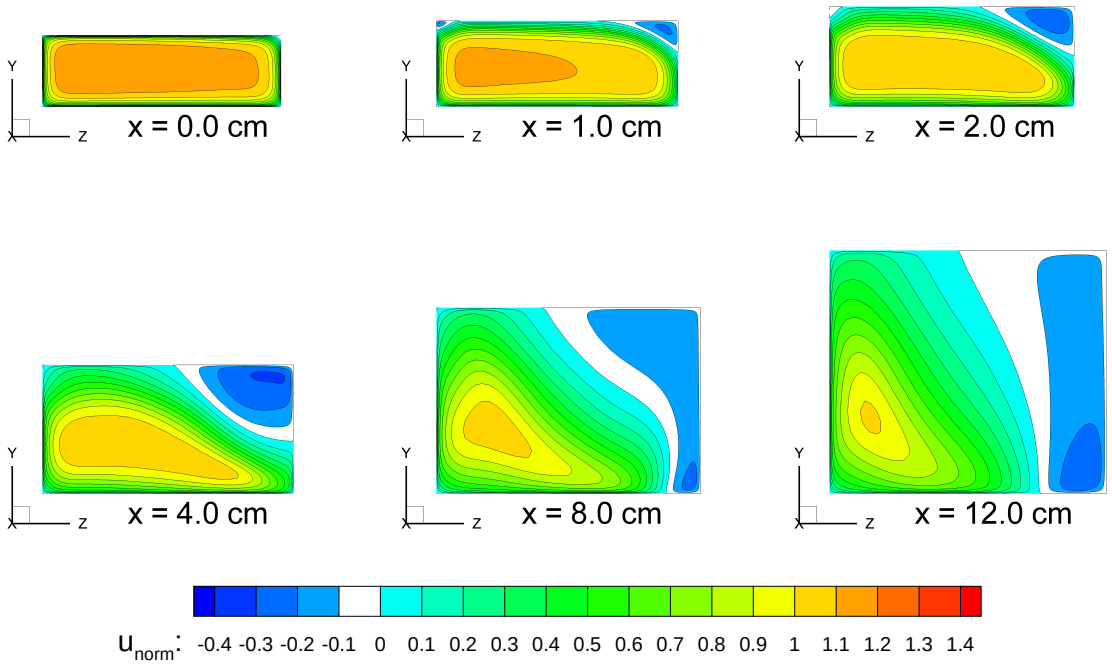

Figure 5.13 Case 3: Contours of Streamwise Velocity with $\overline{v^2} - f$ Model

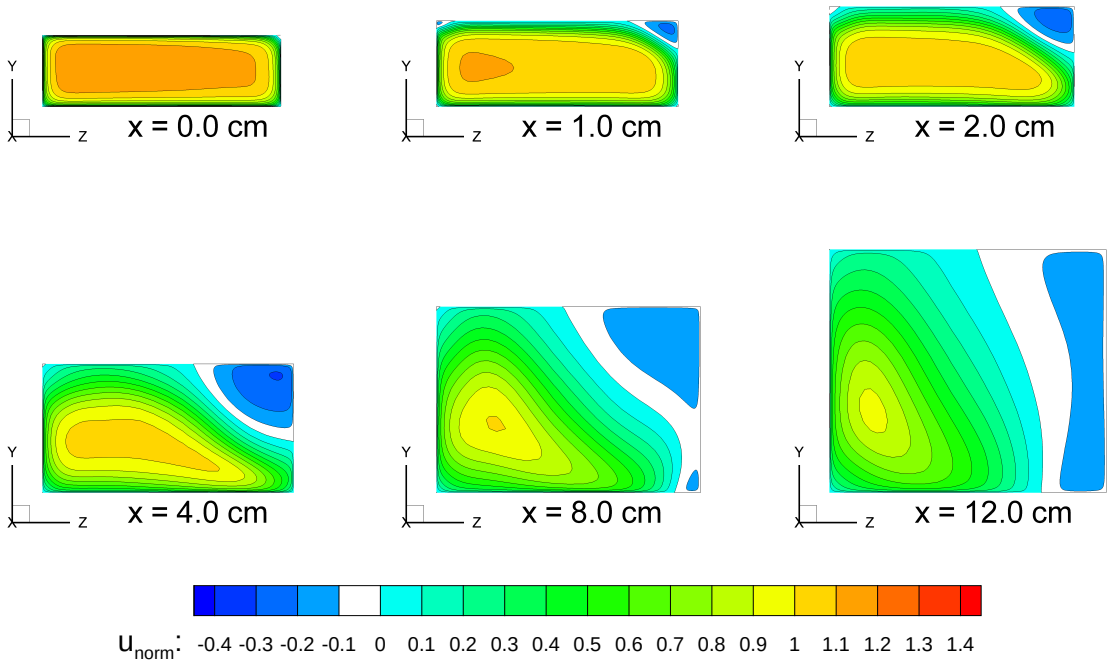

Figure 5.14 Case 3: Contours of Streamwise Velocity with $\zeta - f$ Model

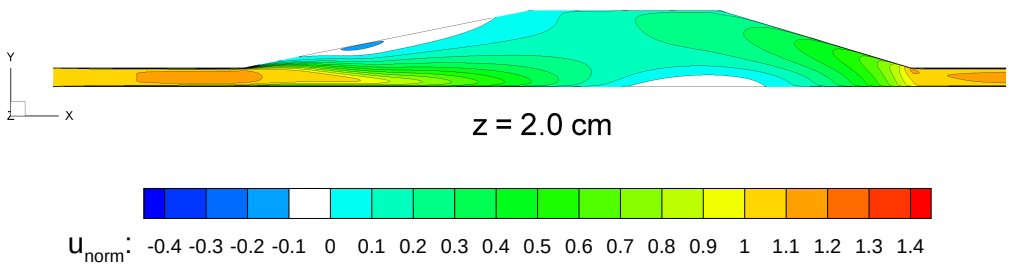

Figure 5.15 Case 3: Contours of Streamwise Velocity at z = 2 cm with $\overline{v^2} - f$ Model

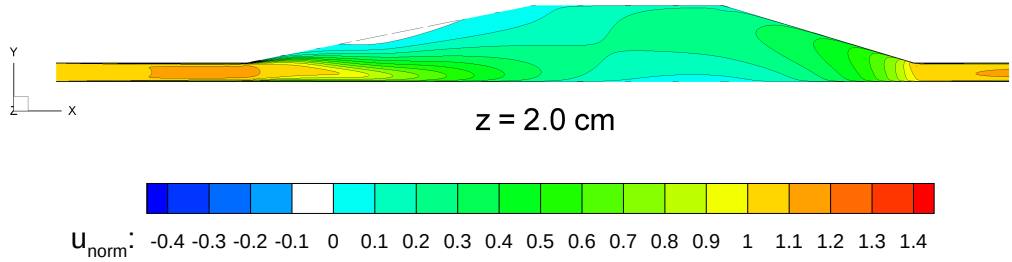

Figure 5.16 Case 3: Contours of Streamwise Velocity at z = 2 cm with $\zeta - f$ Model

top right edge. However, further down the diffuser, the separation transitions toward the right side, opposed to the experimental data which separates on the top side. Also, the strength of the separation is over-predicted by the computational simulations. This discrepancy between experimental and computational results suggests a need for further study to determine the cause of the improper location of separation.

CHAPTER 6. SUMMARY AND DISCUSSION

The objective of this study was to employ two different turbulence models, namely the $\overline{v^2} - f$ model of Durbin and the $\zeta - f$ model of Hanjalić, and to observe their abilities to predict separated flows. Calculations were performed using the NASA Glenn-HT code, a compressible Navier-Stokes solver. Three cases were run using two elliptic relaxation eddy viscosity models, Durbin's $\overline{v^2} - f$ model, and the $\zeta - f$ model of Hanjalić.

The first case, a simple 2-D channel flow simulation, was run using both models. This case was used to validate the implementation of the $\overline{v^2} - f$ and $\zeta - f$ models in Glenn-HT by comparing the results with a separate, 1-D, solution. Both models performed well and predicted the fully developed velocity profile as well as the turbulence quantities accurately.

The second case consisted of a 3-D diffuser which was sloped on a single wall. The results showed that both turbulence models were able to predict the onset of separation along the top right and left edges near the diffuser inlet. The separation transitioned to cover the entire top of the diffuser, and the flow reattached in the straight section following the diffuser.

While the first two cases showed validation and the two models have been shown to accurately predict separation (Ameri, Ajmani 2004 and Durbin 1995), the third case listed in this thesis proved to be difficult to predict using the $\overline{v^2} - f$ and $\zeta - f$ turbulence models. This case consisted of a 3-D diffuser with two sloping walls. The numerical results were compared to the experiment conducted by Cherry *et. al.* (2006). The onset of separation was predicted in the correct location, the top right edge. However, the numerical results show the separation transition towards the right wall, while the experiments show this transition towards the top wall.

This discrepancy between numerical and experimental results suggests a need for further

study. It is recommended that the experiment be validated, and also that the $\overline{v^2} - f$ and $\zeta - f$ models be studied more to determine the cause of this difference. Perhaps the empirical model constants need to be retuned, or additional modifications to the models need to be prescribed. Additionally, it is suggested that this case may describe a weakness in the eddy viscosity approximation. Current research is being performed to run this case with Detached Eddy Simulation (DES) and it is also suggested that a Large Eddy Simulation (LES) code could be tested on this case.

BIBLIOGRAPHY

Ameri, A. A. , Ajmani, K. (2004). Evaluation of Predicted Heat Transfer on a Transonic Blade Using $v^2 - f$ Models. *Proc. of ASME Turbo Expo.*,

Cherry, E. M. , Iaccarino, G. , Elkins, C. J. and Eaton, J. K. (2006). Separated flow in a three-dimensional diffuser: preliminary validation. *Annual Research Briefs, Center for Turbulence Research*, 31–40

Durbin, P. A. (1995). Separated Flow Computations with the $k - \epsilon - v^2$ Model. *AIAA J.*, *33*(4), 659–664.

Durbin, P. A. and Pettersson Reif, B. A. (2001). Statistical Theory and Modeling for Turbulent Flows. Chichester, New York: John Wiley & Sons.

Durbin, P. A. (2004). Turbulence Closure Models for Computational Fluid Dynamics. *Encyclopedia of Computational Mechanics*, *3*, 301–324.

Hanjalić, K. , Popavac, M. , Hadžiabdić, M. (2004) A robust near-wall elliptic-relaxation eddy-viscosity turbulence model for CFD. *Int. J. of Heat and Fluid Flow*, *25*, 1047–1051

Kalitzin, G. (2000) Towards a robust and efficient $v^2 - f$ implementation with application to transonic bump flow. *Annual Research Briefs, Center for Turbulence Research* 291–299

Steinthorsson, E. , Ameri, A. A. , Rigby, D. L. (1999) LeRC-HT The NASA Lewis Research Center General Multi-Block Navier-Stokes Convective Heat Transfer Code

Tannehill, J. C. , Anderson, D. A. , Pletcher, R. H. (1997). Computational Fluid Mechanics and Heat Transfer. Philadelphia, Pennsylvania: Taylor & Francis

Wilcox, D. C. (1994). Turbulence Modeling for CFD. La Canada, California: DCW Industries